Structural diversity of self-cleaving ribozymes

Jin Tang and Ronald R. Breaker*

Department of Molecular, Cellular and Developmental Biology, Yale University, P.O. Box 208103, New Haven, CT 06520-8103

In vitro selection was used to isolate Mg^{2+}-dependent self-cleaving ribozymes from random sequence. Characterization of representative clones revealed the emergence of at least 12 classes of ribozymes that adopt distinct secondary structure motifs. Only one class corresponds to a previously known structural motif, that of the naturally occurring hammerhead ribozyme. Each ribozyme promotes self-cleavage via an internal phosphoester transfer reaction involving the adjacent 2′-hydroxyl group with a chemical rate enhancement of between 10^3- and 10^6-fold greater than the corresponding uncatalyzed rate. These findings indicate that RNA can form a multitude of secondary and tertiary structures that promote cleavage by internal phosphoester transfer. Upon further *in vitro* selection, a class I ribozyme that adopts an ''X motif'' structure dominates over all other ribozymes in the population. Thus, self-cleaving RNAs isolated by *in vitro* selection from random-sequence populations can rival the catalytic efficiency of natural ribozymes.

Four of the seven natural types of ribozymes (1–5) are classified as self-cleaving RNAs that catalyze chain cleavage via an internal phosphoester transfer reaction (6). These ribozymes are found in small pathogenic RNAs such as the delta virus of human hepatitis (7), and in viroid RNAs that are typically associated with various plant diseases (8). Each class of natural ribozymes is distinguished by a highly conserved catalytic core that is formed by assembling both single-stranded regions and secondary structure elements into a precise three-dimensional architecture. The distinctive secondary and tertiary folds of each self-cleaving ribozyme serve to position functional groups and cofactors in space to form an active site that accelerates phosphoester transfer by 10^5- to 10^9-fold over the corresponding uncatalyzed rate of RNA cleavage (6).

There is significant interest in engineering self-cleaving ribozymes to function as sequence-specific RNA cleavage agents for gene inactivation (9). It is of particular interest whether RNA-cleaving ribozymes with enhanced catalytic characteristics can be created that exhibit improved catalytic performance under physiological conditions (10–22). Considering the functional limitations of natural self-cleaving ribozymes, it is apparent that we must begin to explore new RNA structures to create ribozymes with functional and kinetic characteristics that are significantly improved relative to current standards. A number of theoretical arguments (23–26) and experimental results (27, 28) indicate that nucleic acids have tremendous capacity for structure formation and catalytic function. It is known that small RNA structures that are different from those discovered in living systems can facilitate RNA strand scission via internal transesterification (10, 29, 30). However, it has not been determined whether RNA has sufficient structural and chemical diversity to yield new self-cleaving ribozymes that have equal or greater catalytic power compared with natural ribozymes. We set out to conduct a survey of self-cleaving RNA structures that can be derived from a random-sequence population by using *in vitro* selection.

Materials and Methods

Oligonucleotides. Synthetic DNAs and the 21 nt RNA substrate (S21) were prepared as described previously (10). Radiolabeled molecules were prepared using T4 polynucleotide kinase (New England Biolabs) and $[\gamma\text{-}^{32}P]ATP$ according to the manufacturer's directions, purified by a denaturing 20% PAGE, and isolated from the gel by crush-soaking in 10 mM Tris-HCl (pH 7.5 at 23°C), 200 mM NaCl, and 1 mM EDTA. Nucleic acids were precipitated from solution by the addition of sodium acetate to 0.3 mM (pH 5.5) and 2.5 volumes of 100% ethanol.

In Vitro Selection. The RNA population was created by generating a double-stranded DNA template for *in vitro* transcription. SuperScript II reverse transcriptase (RT; GIBCO/BRL) was used to extend 280 pmol of primer 1 DNA (5′-GAAATA-AACTCGCTTGGAGTAACCATCAGGACAGCGACCGTA; region representing 16 possible nearest neighbor combinations is underlined) using 270 pmol of the template DNA (5′- TCT-AATACGACTCACTATAGGAAGACGTAGCCAAN$_{40}$TAC-GGTCGCTGTCCTG; T7 promoter is underlined; N represents an equal mixture of the four nucleotides). The extension reaction was conducted in 50 μl containing 50 mM Tris-HCl (pH 8.3 at 23°C), 75 mM KCl, 3 mM $MgCl_2$, 10 mM DTT, 0.2 mM of each dNTP, and 10 U μl^{-1} RT by incubation at 37°C for 1 h. The double-stranded DNA was recovered by precipitation with ethanol.

The DNA templates were transcribed in 100 μl in the presence of 10 mM $MgCl_2$, otherwise as described previously (10). The reaction was terminated by the addition of 50 μl of 40 mM EDTA and precipitated. The uncleaved precursor RNAs were isolated by denaturing 10% PAGE, recovered from the gel, and stored in deionized water at −20°C until use. In subsequent rounds, double-stranded DNA from PCR was transcribed for 10 min to minimize the loss of RNAs that cleave during transcription.

The initial selection reaction (G0) contained 2,000 pmol of RNA in 400 μl of reaction buffer [50 mM Tris·HCl (pH 7.5 at 23°C), 250 mM KCl, and 20 mM $MgCl_2$] and was incubated at 23°C for 4 h. The reaction was terminated by the addition of EDTA and the RNA was recovered by precipitation. RNA cleavage products were separated by denaturing 10% PAGE, visualized, and quantitated using a Molecular Dynamics PhosphorImager, and the gel region corresponding to the location of the desired RNA cleavage products was excised. The RNA was recovered from the excised gel and the selected RNAs were amplified by RT-PCR as described (10) using primers 1 and 2 (5′- GAATTCTAATACGACTCACTATAGGAAGACG-TAGCCAA; T7 promoter is underlined). The resulting double-stranded DNA was used to transcribe the subsequent RNA population, in which all steps were conducted at approximately one-tenth scale. Representative ribozymes from the populations derived from 6, 9, 12, and 15 rounds of selection were cloned (TOPO-TA cloning kit; Invitrogen) and sequenced (Thermo-Sequenase kit; Amersham Pharmacia).

Artificial Phylogeny Generation. Artificial phylogenies for 20 different sequence classes were generated by reselections upon introduction of mutations. DNA templates corresponding to each class were synthesized with a degeneracy (d) of 0.21 per position (31).

Characterization of Ribozyme Catalytic Function. Initial rate constants for self-cleavage (classes VI and VII) were derived as described elsewhere (32). Rate constants for bimolecular constructs were established using a similar strategy, except that the reactions were allowed to proceed through at least two half-lives of substrate. For single turnover conditions, trace amounts of ^{32}P-labeled substrate were incubated with 500 nM ribozyme. Cleavage sites for unimolecular reactions were determined by incubating 5′ ^{32}P-labeled precursor RNA in selection buffer, separating the products by denaturing 10% PAGE and comparing the gel mobility of the 5′ cleavage fragment to that of each cleavage fragment generated by partial RNA digestion using RNase T1 or alkali as described previously (33). The cleavage site for each bimolecular ribozyme reaction was established by incubating trace amounts of 5′ ^{32}P-labeled substrate RNA with 500 nM ribozyme and comparing the products of ribozyme cleavage, RNase T1 digestion, and alkaline digestion using denaturing 20% PAGE.

Results and Discussion

***In Vitro* Selection of Self-Cleaving Ribozymes.** Isolation of new ribozymes from a population of $\approx10^{14}$ different RNAs was performed using selective amplification (Fig. 1*A*). Each RNA construct includes a 40-nt random-sequence region flanked by domains of defined nucleotide sequence (Fig. 1*B*). The 3′-flanking domain serves as substrate and is designed to experience the loss of nts via ribozyme action, yet still function as a primer-binding site for amplification by RT-PCR. The RNAs were transcribed *in vitro* using T7 RNAP and the uncleaved RNA precursors were isolated by PAGE. The purified RNA precursors were incubated under permissive reaction conditions (see *Materials and Methods*) at 23°C for 4 h. Resulting 5′ cleavage fragments between ≈10 and ≈30 nts shorter than the precursor RNAs were excised and amplified by RT-PCR.

The population of RNAs isolated after six rounds of selection (G6) exhibits a significant level of self-cleavage activity in the presence of Mg^{2+} (Fig. 1*C*). At G6, the major 5′ cleavage products were isolated by PAGE with an effort made to obtain separation at single-nt resolution. The DNA amplification products representing these dominant ribozymes were cloned and sequenced. The remainder of the gel zone, which contained ribozymes of lower copy number that yield 5′ cleavage fragments of different lengths, was used to continue the selective-amplification process. This isolation strategy serves two purposes. First, the ribozymes that produce the major cleavage products, and which presumably dominate the population at G6, can be examined in greater detail. Second, these common sequences are excluded from the subsequent rounds of selection, thereby allowing rare ribozymes to increase in frequency in later populations. Likewise, the main product bands representing the 5′ cleavage fragments at G9, G12, and G15 (Fig. 1*C*) were selectively recovered from the gel and subjected to RT-PCR amplification followed by cloning and sequencing.

Twelve Structural Classes of Self-Cleaving Ribozymes. Sequence analysis of over 100 clones representing RNAs from G6, G9, G12, and G15 revealed as many as 20 distinct ribozyme sequences (data not shown). In some cases, numerous RNAs conformed to a single class of self-cleaving ribozyme based on sequence elements that are common among the related variants. For example, ≈30 clones were identified that can form a common secondary structure with similar core nts that we
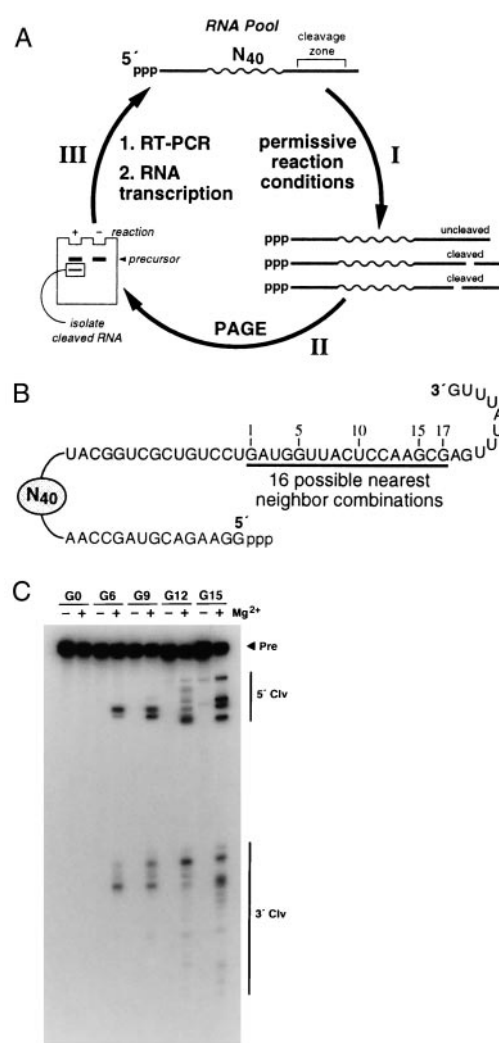

Fig. 1. *In vitro* selection of self-cleaving ribozymes. (*A*) Selection of self-cleaving ribozymes from random-sequence RNA. (*I*) RNAs are incubated under permissive reaction conditions (see text). (*II*) The 5′ fragments of cleaved RNAs are separated from uncleaved precursors by PAGE and (*III*) are amplified by RT-PCR, which introduces a T7 promoter sequence and restores the nucleotides that were lost upon ribozyme cleavage. The resulting double-stranded DNAs are transcribed *in vitro* using T7 RNAP to generate the subsequent population of RNAs. (*B*) RNA construct used to initiate the *in vitro* selection process. N$_{40}$ depicts 40 random-sequence nts. Underlined nucleotides (1–17) identify the region that represents all 16 possible nearest neighbor combinations. (*C*) An autoradiogram of a denaturing 10% PAGE revealing the self-cleavage activities of the starting RNA population (G0) and the populations at G6, G9, G12, and G15 after incubation in the absence (−) or presence (+) of 20 mM Mg^{2+} under otherwise permissive reaction conditions. The locations of the precursor (Pre), 5′ cleavage (5′ Clv), and 3′ cleavage (3′ Clv) fragments are indicated.

defined as class I ribozymes. In other instances, RNAs were isolated that were entirely unique in sequence compared with all other clones. These ''orphan'' sequences were classified independently, as was done with the class II ribozyme (see details below). Ultimately, these 20 different sequence classes were grouped into 12 distinct structural classes that were identified based on the presence of specific sequence elements, secondary structures, and cleavage sites (Fig. 2). Only 1 of the 12 classes (class IX) corresponds to a naturally occurring RNA, the self-cleaving hammerhead ribozyme (1).

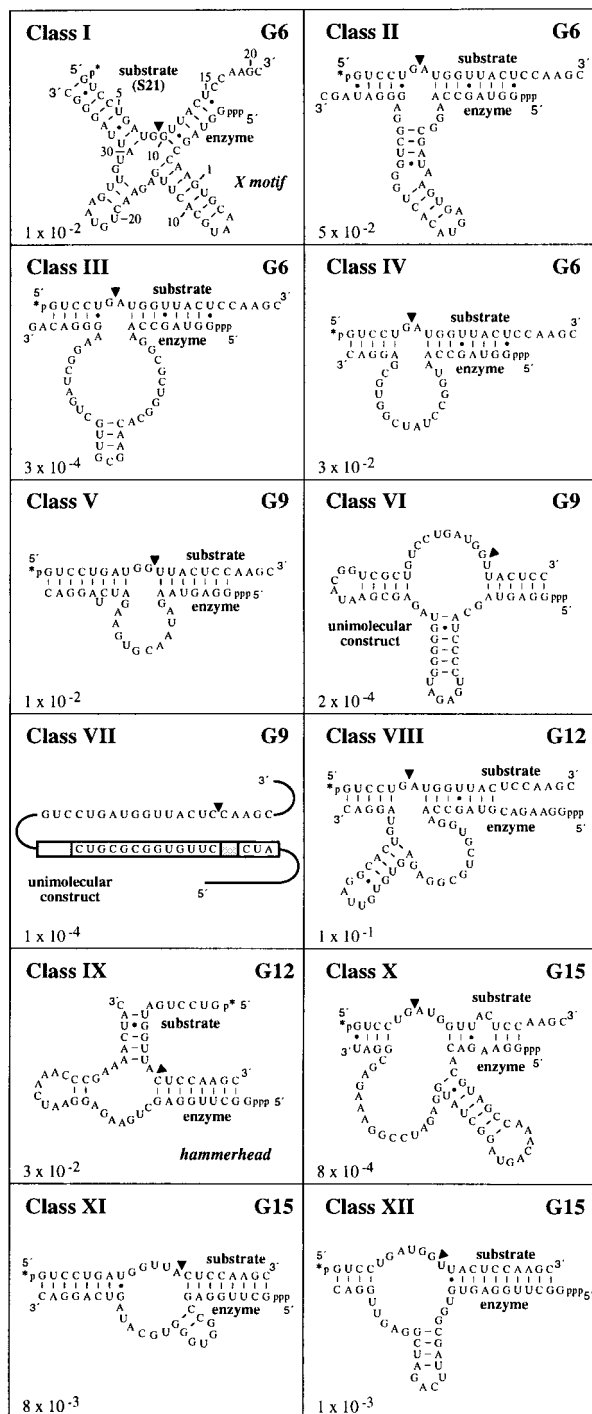For each of the 20 putative sequence classes into which the

Fig. 2. Secondary structure models for 12 classes of self-cleaving ribozymes. Noted for each class is the generation at its first appearance, the rate constant for RNA cleavage (min^{-1}), and the cleavage site (arrowhead). Secondary structure models are based on artificial phylogenetic data (e.g., see Fig. 3A) or otherwise reflect the most stable structure predicted by the Zuker RNA mfold program that is accessible on the internet (44). Putative Watson–Crick base pairing and G·U wobble interactions are represented by dashes and dots, respectively. For most classes, the predicted secondary structure was used as a guide to generate bimolecular ribozyme–substrate complexes that are truncated relative to the original clones. Classes VI and VII were examined as unimolecular constructs because preliminary efforts to generate bimolecular constructs were unsuccessful. For class VII, the boxed regions identify variable (shaded) or conserved nts that reside in the original random-sequence domain.

ribozymes were originally grouped, we conducted three to five rounds of reselection (Fig. 1A) for self-cleavage activity beginning with a population of ribozyme variants based on the nt sequence of a representative clone. After reselection, the mutagenized populations recovered significant levels of self-cleavage activity at which time the variants were identified by cloning and sequencing.

The nucleotide sequences of variant ribozymes were aligned to provide an artificial phylogeny for each class. For example, we observed that the parental sequences of both class I and class II ribozymes undergo substantial mutation without complete disruption of catalytic activity (Fig. 3A). However, the pattern of mutation acquisition in each case is indicative of conserved primary and secondary structures that are important for ribozyme function. The ribozyme variants obtained for class I all retain the prototypic nucleotide sequence at positions 12–16, suggesting that these nts are critical for self-cleavage activity. Nucleotides 8–14, which overlap with the conserved 12–16 nt region, exhibit complementarity to nts within the 3′ primer-binding domain. Moreover, the nts at positions 17–19 and 25–27 are both mutually complementary and highly conserved. This indicates that these latter two sequence elements also might form a hairpin structure with intervening nucleotides 20–24 serving as a connecting loop. Consistent with this interpretation is the observation that mutations within positions 17–19 and 25–27 acquired by a class I ribozyme variant (Fig. 3A, asterisk) allows retention of base complementarity. In addition, the putative loop sequence spanning nucleotides 20–24 tolerates significant mutation as would be expected if the nucleotides in the loop were unimportant for stem formation.

Characteristics of structure formation and conserved sequences evident from the artificial phylogeny for class II ribozymes (Fig. 3A) indicate that it forms a catalytic structure that is distinct from that of class I. Similarly, by analysis of the artificial phylogenetic data for the remaining 18 clones (data not shown), we identified as many as 12 distinct classes of ribozymes (Fig. 2). It is important to note that the structural models depicted in Fig. 2 are not intended to represent confirmed secondary structures. In most cases, limited artificial phylogenetic data coupled with preliminary analyses using a secondary structure prediction algorithm [The secondary structure prediction algorithm RNA mfold can be accessed on the internet (www.ibc.wustl.edu/~zuker/rna/form1.cgi).] were used to derive the models. These depictions should only be considered as starting points for more detailed studies, which are needed to more convincingly establish the secondary structures of each ribozyme class.

Characterization of Bimolecular Ribozyme Reactions. Class I self-cleaving ribozymes form an X-shaped secondary structure (Fig. 2) that locates conserved nts near an unpaired G residue within the substrate. Phosphodiester linkages that reside outside of helical structures are most likely to be targets for ribozyme action because they can more easily adopt an "in-line" geometry that is necessary for internal transesterification (32). Therefore, the structural model indicates that cleavage of S21 should occur at the G residue residing at position 9. Consistent with the proposed "X motif" model is the observation that a bimolecular construct comprised of S21 and a 46-nt enzyme domain (Fig. 2) exhibits Mg^{2+}-dependent cleavage activity 3′ relative to the unpaired G at position 9 (Fig. 3B). Additional phylogenetic and mutational studies have confirmed the importance of the proposed secondary structure for catalytic activity of the X motif (data not shown).

Likewise, a class II construct cleaves S21 between nts 6 and 7 when Mg^{2+} is included in the reaction mixture (Fig. 3B). Considering the different cleavage sites and the apparent differences in secondary structures of class I and class II ribozymes,
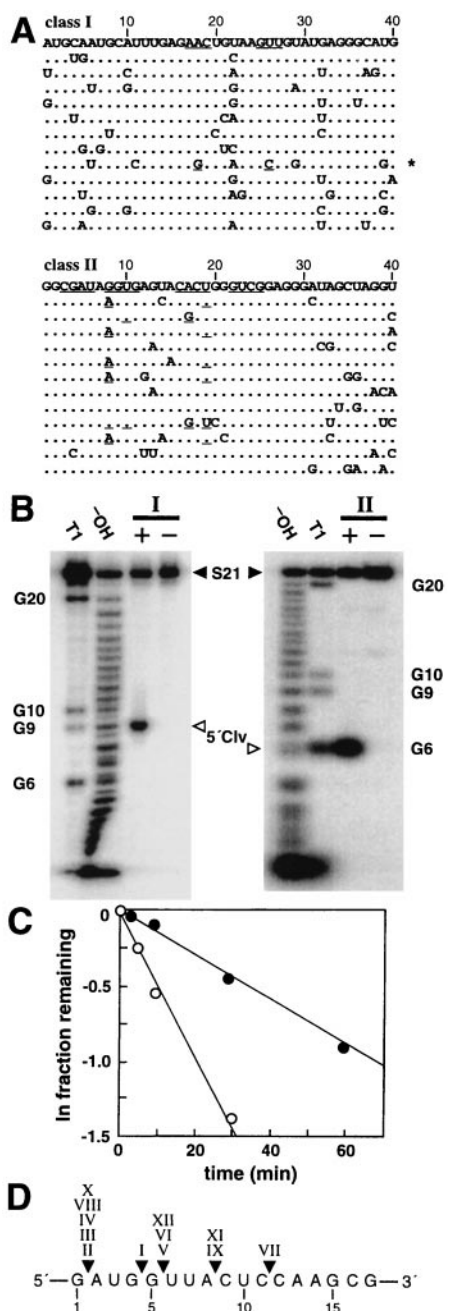
Fig. 3. Characterization of class I and class II self-cleaving ribozymes. (*A*) Sequence variations for artificial phylogenetic analysis are depicted for the nts corresponding to the original random-sequence domain (numbered). Dots indicate no change from the prototype (listed first). Underlined bases retain base complementary. For example, the asterisk identifies a class I ribozyme variant that carries mutations at positions 18 and 26 that retain the ability to base pair. (*B*) Determination of cleavage sites for bimolecular (Fig. 2) class I and class II ribozymes (*Left* and *Right*, respectively). In each case, a trace amount of 21-nt substrate (5′ ³²P-labeled S21) was incubated with (+) or without (−) 500 nM ribozyme under the permissive reaction conditions. The 5′ cleavage fragments (5′ Clv) were separated from uncleaved S21 by denaturing 20% PAGE, and their sizes were compared with S21 5′ cleavage fragments prepared by partial ribonuclease (T1) and partial alkaline (−OH) digests. Class I and class II ribozymes cleave S21 after the G9 and G6 nts, respectively. (*C*) Cleavage reaction profiles for bimolecular class I (filled circles) and class II (open circles) ribozymes (Fig. 2) under the permissive reaction conditions. Observed rate constants for class I and class II ribozymes are 0.01 and 0.05 min⁻¹, respectively, as determined by the negative slope of the lines representing the progression of each reaction. (*D*) Compilation of the cleavage sites of the 12 classes of ribozymes. Numbers identify the nts within the nearest neighbor domain depicted in Fig. 1*B*.

we expect that these RNAs indeed do conform to two distinct catalytic motifs. Bimolecular structures also were tested for 8 of the remaining 10 classes (data not shown). In most instances, ribozyme activity and cleavage patterns are consistent with the proposed secondary structures depicted in Fig. 2. In other cases, more analysis is needed to generate bimolecular constructs (classes VI and VII) or to generate more accurate secondary structure models. The 5′ cleavage fragments produced by each ribozyme comigrate during high-resolution PAGE with RNAs that bear a 2′,3′-cyclic phosphate terminus (Fig. 3*B* and data not shown). This indicates that all ribozymes classes identified in this study most likely cleave RNA via a cyclizing mechanism.

Rate Constants for Prototypic Ribozymes. Rate constants for RNA transesterification were determined for each of the 12 constructs depicted in Fig. 2. For example, both class I and class II constructs produce linear cleavage kinetics through more than one half-life of the substrate (Fig. 3*C*). These representative class I and class II constructs exhibit rate constants of 0.01 and 0.05 min⁻¹, respectively. Similar examinations of the remaining ribozyme constructs (data not shown) reveal that the rate constants for RNA cleavage typically are below 0.05 min⁻¹. In contrast, rate constants for the natural self-cleaving RNAs such as the hammerhead and HDV ribozymes usually range between 0.1 and 10 min⁻¹ (34, 35). For comparison, the uncatalyzed rate of internal RNA transesterification under the selection conditions used is ≈10⁻⁷ min⁻¹ (6). Therefore, even the slowest of constructs depicted in Fig. 2 accelerate RNA cleavage by at least 1,000-fold. The most active prototype construct (class VIII, $k_{obs} = 0.1$ min⁻¹) provides an overall chemical rate enhancement of ≈1 million-fold over the corresponding uncatalyzed rate.

It is important to note that the original selection and the 20 independent reselections were conducted such that even very slow ribozymes were allowed to persist in the population. Under our selection conditions, RNAs that self-cleave with a rate constant $>10^{-3}$ min⁻¹ experience little or no selective disadvantage compared with ribozymes that cleave with infinitely faster cleavage rates. The goal of the reselections was to create variant ribozymes that retained activity so that an artificial phylogeny could be created for each representative RNA. Therefore, the selective pressure applied at this stage also was not sufficient to favor the isolation of ribozymes with rates that rival those of naturally occurring ribozymes.

Diversity of Ribozyme Cleavage Sites. In most cases, substrate-binding specificity is determined by Watson–Crick base pairing between enzyme and substrate. However, the hammerhead ribozyme favors cleavage of the phosphodiester linkage at UH sites, where H represents A, U, or C (11). For comparison, the "10–23" deoxyribozyme isolated by *in vitro* selection (36) exhibits a cleavage site preference that is different from that of the hammerhead. This deoxyribozyme favors cleavage between unpaired purine-pyrimidine dinucleotides (37). Given these precedents, we expect that new ribozyme and deoxyribozyme motifs might also show significant preferences for cleavage site composition.

To maximize the diversity of ribozymes that could be isolated by our selection scheme, we included the nearest neighbor domain depicted in Fig. 1*B*. This domain provides a comprehensive sampling of all 16 dinucleotides, thereby offering a greater diversity of cleavage sites than would be present in most substrate domains of arbitrary sequence composition. We find that the 12 classes of ribozymes examined in this study cleave at five different locations within the nearest neighbor domain (Fig. 3*D*). As predicted from the RNA cleavage pattern depicted in Fig. 1*C*, ribozymes isolated from the G6 population (classes I-IV) cleave at two sites, both near the 5′ end of this domain. Similar correspondence between cleavage patterns and cleavage
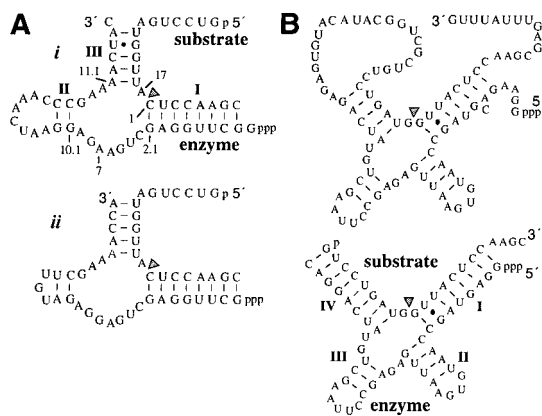
Fig. 4. Comparison of the secondary structures of two hammerhead ribozymes and the dominant X motif. (*A*) Variant hammerheads *i* and *ii* isolated from the G12 and G15 populations, respectively. Stem elements and nts in *i* are numbered according to the nomenclature defined by Hertel *et al.* (45) for hammerhead ribozymes. (*B*) The dominant ribozyme isolated after a total of 25 rounds of *in vitro* selection conforms to the X motif. This ribozyme can be reorganized in a bimolecular construct with a 43-nt enzyme and S21 substrate. Arrowheads identify the sites of ribozyme-mediated cleavage.

Fig. 5. Cleavage site versatility of the X motif. (*A*) Three 43-nt RNAs carrying the conserved features of the X motif ribozyme but differing in base pairing potential of arms I and IV were generated by *in vitro* transcription and targeted to cleave a 51-nt RNA. The lines represent nts within binding arms I and IV that are complementary to the X-E1 target site (arrow). Likewise, ribozymes X-E2 and X-E3 carry the arms that allow unique base pairing (dashes) with their corresponding target sites. (*B*) Cleavage of the RNA substrate (sub) upon incubation with three engineered ribozymes. Substrate (trace, 5' ^{32}P-labeled) is not cleaved when incubated under *in vitro* selection conditions for 1 h in the absence of ribozyme (lane 1), but undergoes site-specific cleavage (clv) at the expected locations when incubated with 500 nM ribozymes X-E1, X-E2, and X-E3 (lanes 2–4, respectively).

site selection is observed with ribozymes isolated from subsequent rounds. However, ribozymes from G12 and G15 that generate the largest 5' cleavage fragments are not representative of new cleavage sites near the 3' end of the nearest neighbor domain. For example, classes VIII and X cleave at the same site as three classes of ribozymes that were isolated in G6. We found that VIII and X accumulated insertions in the original N_{40} domain that yield longer 5' cleavage fragments despite processing at sites that are also used by other ribozymes (data not shown). It is not clear, however, whether the most common cleavage site (GA) is intrinsically favorable.

Emergence of the Hammerhead Ribozyme Motif. Given that the hammerhead has low structural and sequence complexity (38), we expected that numerous variants of this ribozyme would be represented in the initial RNA pool. Indeed, among the >100 clones examined, we identified two sequences (Fig. 4A, variants *i* and *ii*) that conform to the consensus sequence and secondary structure of the hammerhead motif. However, both hammerhead variants differ from the established consensus sequence and structure that is important for full catalytic activity (10, 16). Variants *i* and *ii* carry an A and G, respectively, at position 7 of the catalytic core. Although the ribozyme can tolerate nt variation at position 7, the most active hammerhead ribozyme variants typically carry a U or C residue at this position (10, 39). Moreover, the sequence and stability of stem II is known to be a critical determinant of ribozyme activity (12, 40–42). The hammerhead variants isolated in this study have a relatively short base-paired element that forms stem II, suggesting that this structure might not be optimal for ribozyme function. Not surprisingly then, hammerhead *i* (Fig. 2, class IX) was found to exhibit an observed rate constant that is ≈30-fold lower than that of typical hammerhead ribozymes.

X Motif Challenges the Catalytic Efficiency of the Hammerhead Ribozyme. Nearly all ribozyme constructs derived from the reselections (Fig. 2) exhibit rate constants for RNA cleavage that are below the maximum values obtained for natural ribozymes. This observation brings into question whether new motifs can even approach the catalytic efficiency of natural ribozymes. Until this point, our efforts have been directed toward the identification and confirmation of new structural motifs for
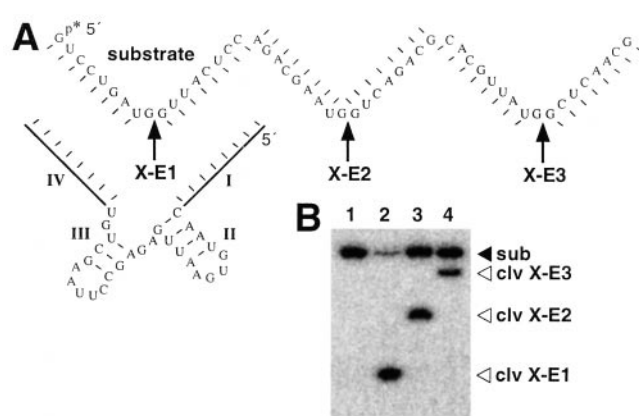
self-cleaving ribozymes. Therefore, the selection reactions intentionally were conducted under exceedingly permissive conditions such that even highly defective variants of new motifs could ultimately be identified by cloning and sequencing. Likewise, reselections were conducted under equally permissive conditions for artificial phylogeny construction, and not necessarily to produce superior catalysts. Indeed, none of the 20 reselections conducted, including that which was carried out using a mutagenized population derived from hammerhead *i*, provided variant ribozymes that exhibit kinetic characteristics that match natural ribozymes.

Therefore, we set out to enrich for ribozyme variants whose rate constants were significantly higher than that of the general population. We pooled samples from G6, G9, G12, and G15 and subjected the RNAs to additional rounds of *in vitro* selection as described in Fig. 1*A*, but where decreasing reaction times (as low as 5 sec) were used to favor the isolation of the fastest ribozymes in the population. After 10 rounds of selection, we found that the RNA population undergoes ≈6% cleavage upon incubation for 5 sec. Surprisingly, only a single 5' cleavage fragment was observed, indicating that a single class of relatively fast ribozymes (k_{obs} ≈0.7 min^{-1}) had come to dominate the RNA population. Indeed, cloning and sequencing revealed that the population was comprised primarily of a single RNA sequence variant (Fig. 4*B*) of the original X motif ribozyme (Fig. 2, class I).

A bimolecular construct based on this RNA (Fig. 4*B*) exhibits a k_{obs} of ≈0.2 min^{-1} under single turnover conditions, which corresponds to a 20-fold improvement over the corresponding class I construct depicted in Fig. 2. The maximum rate constant expected for optimal hammerhead ribozymes (≈1 min^{-1}) remains severalfold greater than that measured for the bimolecular version of the improved X motif depicted in Fig. 4*B*. However, the X motif can be made to catalyze RNA cleavage with a k_{obs} of ≈10 min^{-1} under optimized reaction conditions. Therefore, we conclude from these findings that other small RNA motifs can form RNA-cleaving structures that compare favorably in catalytic rate enhancement with that of natural ribozymes.

Although ribozymes such as the hammerhead might be among the most active small motifs, our data indicate that it is possible to isolate new ribozymes that have comparable or even superior kinetic characteristics.

Prospects for the Therapeutic Application of New Ribozymes. Two parameters are of paramount concern when evaluating new ribozymes for their potential use as versatile and efficient agents for specifically targeting RNAs for destruction. First, candidate ribozymes should catalyze RNA cleavage with an efficiency that offers a distinct advantage over that of other anti-RNA compounds such as antisense oligonucleotides. RNA-cleaving molecules such as the hammerhead ribozyme and the 10–23 deoxyribozyme cleave with a rate constant of ≈ 1 min^{-1}, and both exhibit significant anti-mRNA activity *in vivo* (e.g., ref. 43). The X motif therefore appears to have the catalytic power under our *in vitro* selection conditions to cleave RNA on a time scale that is relevant to biology.

Second, a therapeutic RNA-cleaving motif should be amenable to engineering strategies that alter target site specificity. For example, the substrate specificity of the hammerhead can be altered to cleave different RNA sequences by re-engineering Watson–Crick pairing between ribozyme and substrate. Likewise, the X motif can be engineered to cleave with high specificity at distinct RNA target sites simply by altering stems I and IV to uniquely hybridize to the substrate sequence of interest (Fig. 5). Thus, classes I–V and VIII all appear to be attractive candidates for further development as anti-RNA agents.

Conclusions

As many as 12 different self-cleaving ribozyme motifs that catalyze site-specific RNA cleavage have been isolated from a small population of random-sequence RNAs. We expect that a comprehensive effort which incorporates larger populations of random-sequence RNAs would yield far more self-cleaving ribozyme structures than were identified in this study. Also, a more comprehensive cloning and sequencing effort would likely reveal many new ribozyme motifs that are present in our selected populations at lower frequencies. We speculate that there must be a large number of undiscovered RNA structures that can accelerate the site-specific cleavage of RNA with chemical rate constants that are of biological relevance.

Many of the prototypic ribozyme constructs examined in this study are not likely to be optimal for catalytic function. Therefore, further improvements in structure and function could provide new ribozymes for use in various anti-RNA applications. The finding that 1 of the 12 ribozymes isolated during this study was the naturally occurring hammerhead ribozyme highlights the possibility that other motifs presented herein might already play roles in biological systems. Preliminary analysis indicates that the X motif has a catalytic rate constant that is significant on a biological time scale. Moreover, given that the sequence and structural complexity of several new ribozymes reported in this study are equivalent to that of the hammerhead, we speculate that self-cleaving RNAs conforming to these new classes might already exist in nature.

1. Symons, R. H. (1992) *Annu. Rev. Biochem.* **61,** 641–671.
2. Cech, T. R. (1990) *Annu. Rev. Biochem.* **59,** 435–461.
3. Michel, F. & Ferat, J.-L. (1995) *Annu. Rev. Biochem.* **64,** 453–461.
4. Frank, D. N. & Pace, N. R. (1998) *Annu. Rev. Biochem.* **67,** 153–180.
5. Zimmerly, S., Guo, H., Eskes, R., Yang, J., Perlman, P. S. & Lambowitz, A. M. (1995) *Cell* **83,** 529–538.
6. Li, Y. & Breaker, R. R. (1999) *J. Am. Chem. Soc.* **121,** 5364–5372.
7. Lai, M. M. (1995) *Annu. Rev. Biochem.* **64,** 259–286.
8. Symons, R. H. (1999) in *Comprehensive Natural Products Chemistry,* eds. Barton, D., Nakanishi, K. & Meth-Cohn, O., Vol. 6, pp.168–187.
9. Christoffersen, R. E. & Marr, J. J. (1995) *J. Med. Chem.* **38,** 2023–2037.
10. Tang, J. & Breaker, R. R. (1997) *RNA* **3,** 914–925.
11. Vaish, N. K., Heaton, P. A., Fedorova, O. & Eckstein, F. (1998) *Proc. Natl. Acad. Sci. USA* **95,** 2158–2162.
12. Conaty, J., Hendry, P. & Lockett, T. (1999) *Nucleic Acids Res.* **27,** 2400–2407.
13. Nakamaye, K. L. & Eckstein, F. (1994) *Biochemistry* **33,** 1271–1277.
14. Ishizaka, M., Ohshima, Y. & Tani, T. (1995) *Biochem. Biophys. Res. Commun.* **214,** 403–409.
15. Thomson, J. B., Sigurdsson, S. T., Zeuch, A. & Eckstein, F. (1996) *Nucleic Acids Res.* **24,** 4401–4406.
16. Vaish, N. K., Heaton, P. A. & Eckstein, F. (1997) *Biochemistry* **36,** 6495–6501.
17. Berzal-Herranz, A., Joseph, S. & Burke, J. M. (1992) *Genes Dev.* **6,** 129–134.
18. Joseph, S., Berzal-Herranz, A., Chowrira, B. M., Butcher, S. E. & Burke, J. M. (1993) *Genes Dev.* **7,** 130–138.
19. Berzal-Herranz, A., Joseph, S., Chowrira, B. M., Butcher, S. E. & Burke, J. M. (1993) *EMBO J.* **12,** 2567–2574.
20. Joseph, S. & Burke, J. M. (1993) *J. Biol. Chem.* **268,** 24515–24518.
21. Kawakami, J., Kumar, P. K. R., Suh, Y.-A., Nishikawa, F., Kawakami, K., Taira, K., Ohtsuka, E. & Nishikawa, S. (1993) *Eur. J. Biochem.* **217,** 29–36.
22. Nishikawa, F., Kawakami, J., Chiba, A., Shirai, M., Kumar, P. K. R. & Nishikawa, S. (1996) *Eur. J. Biochem.* **237,** 712–718.
23. White, H. B., III (1976) *J. Mol. Evol.* **7,** 101–104.
24. Benner, S. A., Ellington, A. D. & Tauer, A. (1989) *Proc. Natl. Acad. Sci. USA* **86,** 7054–7058.
25. Breaker, R. R. (1997) *Nat. Biotechnol.* **15,** 427–431.
26. Yarus, M. (1999) *Curr. Opin. Chem. Biol.* **3,** 260–267.
27. Breaker, R. R. (1997) *Chem. Rev.* **97,** 371–390.
28. Robertson, M. P. & Ellington, A. D. (1999) in *Comprehensive Natural Products Chemistry*, eds. Barton, D., Nakanishi, K. & Meth-Cohn, O., Vol. 6, pp. 115–148.
29. Pan, T. & Uhlenbeck, O. C. (1992) *Biochemistry* **31,** 3887–3895.
30. Williams, K. P., Ciafre, S. & Tocchini-Valentini, G. P. (1995) *EMBO J.* **14,** 4551–4557.
31. Breaker, R. R. & Joyce, G. F. (1994) *Trends Biotechnol.* **12,** 268–275.
32. Soukup, G. A. & Breaker, R. R. (1999) *Proc. Natl. Acad. Sci. USA* **96,** 3584–3589.
33. Soukup, G. A. & Breaker, R. R. (1999) *RNA* **5,** 1308–1325.
34. Fedor, M. J. & Uhlenbeck, O. C. (1992) *Biochemistry* **31,** 12042–12054.
35. Thill, G., Vasseur, M. & Tanner, N. K. (1993) *Biochemistry* **32,** 4254–4262.
36. Santoro, S. W. & Joyce, G. F. (1997) *Proc. Natl. Acad. Sci. USA* **94,** 4262–4266.
37. Santoro, S. W. & Joyce, G. F. (1998) *Biochemistry* **37,** 13330–13342.
38. Forster, A. C. & Symons, R. H. (1987) *Cell* **49,** 211–220.
39. Ruffner, D. E., Stormo, G. D. & Uhlenbeck, O. C. (1990) *Biochemistry* **29,** 10695–10702.
40. Tuschl, T. & Eckstein, F. (1993) *Proc. Natl. Acad. Sci. USA* **90,** 6991–6994.
41. Long, D. M. & Uhlenbeck, O. C. *Proc. Natl. Acad. Sci. USA* **91,** 6977–6981.
42. Tang, J. & Breaker, R. R. (1997) *Chem. Biol.* **4,** 453–459.
43. Warashina, M., Kuwabara, T., Nakamatsu, Y. & Taira, K. (1999) *Chem. Biol.* **6,** 237–250.
44. Zuker, M. (1998) *Science* **244,** 48–52.
45. Hertel, K. J., Pardi, A., Uhlenbeck, O. C., Koizumi, M., Ohtsuka, E., Vesugi, S., Cedergren, R., Eckstein, F., Gerlach, W. L., Hodgson. R. & Symons, R. H. (1992) *Nucleic Acids Res.* **20,** 3252.

BIOCHEMISTRY